

Anomalous Polarization in One-dimensional Aperiodic Insulators

A. Moustaj,¹ J.P.J. Krebbekx,¹ and C. Morais Smith¹

¹*Institute of Theoretical Physics, Utrecht University,
Princetonplein 5, 3584CC Utrecht, The Netherlands.*

(Dated: April 24, 2024)

By implementing a charge pumping scheme for one-dimensional aperiodic chains, we confirm the existence of topological phases in these systems whenever their finite-size realizations admit inversion symmetry. These phases are usually characterized by an anomalous edge response as a result of the bulk-boundary correspondence. We show that these signatures are all present in various chains, each representing a different class of structural aperiodicity: the Fibonacci quasicrystal, the Tribonacci quasicrystal, and the Thue-Morse chain. More specifically, we calculate three quantities: the Berry phase of the crystalline approximation of the finite-size systems, the polarization response to an infinitesimal static and constant electric field in systems with open boundary conditions, and the degeneracy of the entanglement spectrum. We find that all of them provide signatures of a topologically nontrivial phase.

I. INTRODUCTION

Electronic band theory is a cornerstone of condensed-matter physics, usually grounded on the crystalline structures found in solid-state materials. The latter allows one to use crystal cells to construct Bloch Hamiltonians, which are much simpler to deal with than their real-space counterparts. By using these Bloch band structures, a well-established theoretical framework for topological insulators (TI's) and superconductors has been developed during the last decades [1–3]. However these concepts are not restricted to periodic systems, as topologically nontrivial insulating states have also been found in amorphous materials and disordered systems [4, 5].

One of the main properties of TI's is the bulk-boundary correspondence, which implies the existence of robust in-gap edge modes in one dimension (1D) and *gapless* boundary states in two and higher dimensions (2D and 3D). The physical response of such systems can be probed by the application of external perturbations, after which one finds either conducting channels at the boundary of an otherwise insulating bulk in 2D and 3D, or an anomalous polarization response and fractional corner charges in 1D [6–9]. Another class of 1D systems for which quantized boundary responses are possible are superconductors. A prime example where this happens is the Kitaev chain [10], which hosts Majorana edge states.

In the case of periodic crystals, the nontrivial topology of 2D and 3D TI's is generally attributed to the nonexistence of a complete set of exponentially localized Wannier functions, also known as an *obstruction to Wannierization* [11]. As a consequence, a topologically nontrivial state cannot be adiabatically connected to an atomic limit in which electrons occupy maximally localized Wannier states. In 1D, however, it is known that localized Wannier bases can always be constructed, such that there cannot be any topological obstruction [12]. Nevertheless, topologically nontrivial insulators,

with anomalous polarization and fractional boundary charges, in fact exists. These phases are known to be equivalent to *obstructed atomic limits*, which are not adiabatically connected with *trivial atomic limits* [13]. In order for this to happen, crystalline symmetries must be imposed on the system. The only possible such symmetry in 1D is inversion, forcing the polarization density of the system to be quantized at 0 or 1/2 (in units where $e = 1$) [8, 9]. In turn, it is possible to relate the bulk topological invariant of a chiral-symmetric (or equivalently sublattice-symmetric) 1D system to its quantized polarization [14], and therefore understand the physical implications of the nontrivial topology of a 1D insulator. Namely, there exists an anomalous boundary response in the obstructed atomic phase in the form of a quantized polarization resulting from the pile up of fractionalized charges at the edges. The paradigmatic example of such a phase is realized in the Su-Schrieffer-Heeger (SSH) model [6].

Given that most toy models realizing such phases are typically periodic crystals, one wonders whether aperiodic 1D systems can also host some sort of obstructed atomic limits. Intense efforts have been made in the last decade to understand whether such nontrivial topological phases could also exist in 1D quasicrystalline systems [15–18]. It was shown that the gapped spectra of quasicrystalline Hamiltonians carry nontrivial signatures of topology. For example, a typical quasicrystal carries gap labels which have a topological origin and can be understood from K-theory [19]. These topological indices have also been linked with the pumping of boundary states [16, 20]. However, the question remains whether these observations constitute genuine signatures of anomalous boundary physics, related to bulk properties by means of a bulk-boundary correspondence. In other words, do the topological labels observed in noncrystalline systems in 1D imply the existence of an electronically insulating topological phase, which is adiabatically connected to some type of obstructed atomic limit, and to which anomalous boundary physics can they be linked to? To

the best of our knowledge, this question has so far not been fully addressed, and we show in this work that it is indeed possible to find such phases for finite-size realizations of aperiodic systems. In order to reach this conclusion, we will use typical probes for anomalous edge responses, such as the Berry phases of crystalline approximants, the anomalous polarization responses to external static electric fields and entanglement spectrum (ES) degeneracies. The systems that we will consider are the Fibonacci chain, the Tribonacci chain, and the Thue-Morse chain. By performing the adiabatic quantized charge pumping protocol proposed in Ref. [21] for the Fibonacci chain, we show that multilevel pumping also works for at least two other aperiodic modulations: the Tribonacci sequence and the Thue-Morse sequence. We then identify the points in time where the Berry phase of these approximants is exactly 0 or π . These turn out to be the points where the boundary states of open systems are degenerate. This inversion-symmetric realization is then used to show that the systems have an anomalous polarization response of $\mathcal{P} = 0.5$, which is due to the degeneracy of the edge modes. The results are further corroborated by calculations of the entanglement spectrum, which shows a double degeneracy each time that a system has Berry phase of π .

This work is structured as follows. In Section II, we briefly review the classification scheme of topological insulators and the associated physical observables that result from the bulk-boundary correspondence in 1D. This is followed in Section III by a short overview of aperiodic systems. In Section IV, we recall recent literature results on topological states of 1D quasicrystalline systems, and contextualize them with respect to the classification scheme. That is, we discuss how the results can be interpreted in terms of 2D topologically insulating phases. In Section V, we present the charge-pumping protocol and the results obtained for the various aperiodic systems considered in this work. In Section VI, the results obtained from probing the different physical signatures of 1D TI's in three different classes of aperiodic systems are discussed. We show that all the signatures that one should expect to see are present in these systems. Finally, in Section VII, we conclude with a summary and outlook.

II. SIGNATURES OF 1D TOPOLOGICAL INSULATORS

Here, we briefly review the concept of a topological insulator. We will focus on a very specific setup of gapped noninteracting systems of fermions. The theoretical understanding of topological insulators is based on their classification in terms of anti-unitary symmetries and dimensionality. This classification is equivalent to that of random matrices, and is known as the Altland-Zirnbauer classification, or the ten-fold way [22].

The most general statement that can be made concerning symmetry-protected topological states of matter is that they are ground states of a many-body system that are adiabatically distinct from a trivial product of single-particle states, also called the *trivial atomic limit*. By using K-theory, it has been shown that the generalized homotopy group of a Bloch Hamiltonian taking values in the d -dimensional Brillouin zone (BZ) T^d and belonging to a certain classifying space R_q can be written as [23]

$$\pi(T^d, R_q) = \pi_0(R_{q-d}) \bigoplus_{s=0}^{d-1} \pi_0(R_{d-s}).$$

The classifying spaces R_q are the sets of real symmetric matrices under the constraint of anti-unitary symmetries, and with eigenvalues ± 1 . They are labeled by the integer $q \bmod 8$, and correspond to the 8 real Cartan classes. A similar equation can be posed for the complex classifying spaces C_q , corresponding to the set of Hermitian matrices labeled by the integer $q \bmod 2$, and associated with the 2 complex Cartan classes. The first part of this equation, namely $\pi_0(R_{q-d})$ is what appears in the ten-fold classification. The second part is attributed to unitary symmetries, which allow point-group symmetries to protect topologically nontrivial states as well. A consequence of this is the existence of topological crystalline insulators [13], which are nontrivial topological states protected by crystalline symmetries of the lattice. Now, let us review some of the tools that have been developed to characterize topological states of matter in 1D.

a. Wilson loops. Wilson loops are gauge-invariant operators that originated in particle physics [24]. They arise in condensed-matter theory when submitting a system to an adiabatic evolution through a non-contractible loop in parameter space. They are intimately linked to the Berry phase and its geometric interpretation through the Berry connection [25]. The latter allows for parallel transport of eigenstates of the Hamiltonian living in the subspace of occupied states. It provides a means to probe the intrinsic curvature of a $U(N)$ principal bundle by considering the holonomy

$$\mathcal{W} = \mathcal{P} \exp \left[i \oint_{\mathcal{C}} \mathbf{A}(\boldsymbol{\lambda}) \cdot \boldsymbol{\lambda} \right],$$

where \mathcal{P} denotes the path ordering procedure defining the exponential of an integral of an operator and \mathcal{C} is a closed path in parameter space, i.e. $\boldsymbol{\lambda}(0) = \boldsymbol{\lambda}(\tau)$. \mathcal{W} is known as the Wilson loop operator, and by choosing a specific differentiable basis, we can express the Berry connection $\mathbf{A}(\boldsymbol{\lambda})$ (and hence the Wilson loop) as

$$\mathbf{A}_{mn}(\boldsymbol{\lambda}) = \langle \psi_m(\boldsymbol{\lambda}) | i \partial_{\boldsymbol{\lambda}} | \psi_n(\boldsymbol{\lambda}) \rangle.$$

The data contained in the holonomy reveals the failure of states to be transported back to themselves after a closed-loop evolution in parameter space. For a generic state under adiabatic evolution, this is precisely the Berry phase acquired on top of the usual dynamical phase.

In order to see how this formulation allows to define topological invariants, we consider a two-band, one dimensional periodic crystal, for which the insulating ground state consists of a filled valence band, separated from the conduction band by a gap. The paradigmatic model for such a system is the SSH chain [6]. It will be used as a benchmark in Section VI to compare the results on aperiodic systems. The Hamiltonian is given by

$$H_{\text{SSH}} = -g \sum_{n=1}^{2N} [1 - (-1)^n \delta] c_n^\dagger c_{n+1} + \text{h.c.}, \quad (1)$$

where g is the hopping amplitude, δ is the dimerization parameter, and N the amount of unit cells. The parameter space is the 1D BZ (topologically denoted as the circle S^1). We can define the Berry phase of the valence band eigenstate $|\psi_-(k)\rangle$ with respect to the BZ as

$$\gamma = i \oint_{\text{BZ}} dk \langle \psi_-(k) | \partial_k | \psi_-(k) \rangle.$$

It turns out that under the constraint of inversion symmetry in 1D, the Berry phase (also called Zak phase in this case) must be quantized to either 0 or π [8]. This is because $k \rightarrow -k$ under inversion, which reverse the path of the contour in the integral, while the integrand remains invariant. Hence, we have

$$e^{i\gamma} = e^{-i\gamma} \rightarrow \gamma = 0, \pi.$$

Additionally, since the Hamiltonian also exhibits chiral symmetry $\mathcal{S}H\mathcal{S}^{-1} = -H$, with \mathcal{S} denoting the chiral symmetry operator, an additional protection of this phase takes place if the boundary modes are at $E = 0$. This spectral symmetry allows one to define the winding number [14]

$$\nu = \int \frac{dk}{4\pi i} \text{Tr} [\mathcal{S} \partial_k \log H(k)],$$

which can be shown to be related to the quantized Berry phase of an inversion symmetric system through $\gamma = \pi\nu$. For $\delta < 0$, the SSH chain is in the topological phase, and has two boundary zero modes. The winding number can be calculated exactly and is $\nu = 0$ ($\nu = 1$) for $\delta > 0$ ($\delta < 0$).

b. Bulk-Boundary Correspondence. The quantization of the winding number has an interesting physical meaning, which eventually takes the form of a bulk-boundary correspondence. The reason is that the spectrum of the Wilson-loop operator is equivalent to the spectrum of the projected position operator $\hat{\mathcal{P}}\hat{x}\hat{\mathcal{P}}$, where $\hat{\mathcal{P}}$ projects onto the fermionic ground state [26, 27]. The expectation value of the projected position operator indicates how charge is distributed within a unit cell. In the case of an inversion symmetric insulator, $\gamma = 0$ corresponds to a charge distribution around the center of a unit cell, while $\gamma = \pi$ corresponds to a charge distribution at its boundaries. The eigenvalues of the polarization density operator are related to the Berry phase

through the following equation [26, 27]

$$P = \frac{1}{2\pi i} \log \mathcal{W} = \begin{cases} 0, & \text{if } \gamma = 0, \\ \frac{1}{2}, & \text{if } \gamma = \pi. \end{cases} \quad (2)$$

This means that if one takes a finite system composed of an integer amount of unit cells, so as to keep the inversion symmetry intact, one finds half charges located at the boundaries of the system. The infinitesimal response to an external electric field should reflect this property. If a system does not preserve inversion symmetry, then the polarization density can take any value. This means that it is only possible to obtain quantized Berry phases, and therefore a quantized boundary response when inversion symmetry is present in 1D.

We can further understand these topological properties in terms of adiabatic deformations to different atomic limits: the trivial and the obstructed atomic limit. They are the only two different elementary band representations possible for systems possessing inversion symmetry [13]. The half charges that result from such a situation are also intimately related to the concept of a filling anomaly, in which a certain amount of degenerate single-particle eigenstates lie at the Fermi energy [26]. Finally, this last point allows for another useful formulation of the topological phase through the ES. A robust signature of this filling anomaly is a degenerate ES of the insulator's many-body ground state [28].

Having understood these points, one then wonders how to put in perspective the bulk-boundary correspondence [29] developed in the literature for the various quasicrystalline platforms.

III. APERIODIC SYSTEMS

Aperiodic sequences have attracted a considerable amount of interest since their first applications in the study of physics systems. For example, by studying spin chains under the influence of aperiodic modulations, it was understood that depending on the fluctuations of the aperiodic sequence, it is possible to access different universality classes of quantum phase transitions [30–32]. Later on, the properties of single-particle Hamiltonians on one dimensional quasicrystals were investigated using various techniques, such as renormalization schemes and trace maps. Amongst many interesting results, it was discovered that the spectrum is singular continuous and the eigenstates are neither localized nor delocalized, but are *critical* and exhibit multifractal behavior [33–37]. More recently, theoretical and experimental works have shown that: i) it is possible to observe topological charge pumping in quasiperiodic chains [16, 20, 38]; ii) that the critical eigenstates are robust against local impurities [39]; iii) That the critical states emerge from a cascade of localization-delocalization transitions [40]; iv) coupling of quasicrystalline chains may result in the simultaneous existence of critical and extended eigenstates

[41]. It was also shown that it is possible to control edge states by manipulating local structures in various aperiodic systems, due to the presence of local symmetries [42]. Aperiodic modulations may have other interesting implications on physical systems. We refer the reader for a comprehensive review to Refs. [43, 44]

Before we delve into the nature of topological phases in 1D quasicrystalline insulators, we shall give a brief overview of some aperiodic systems. Contrary to their periodic counterparts, these systems do not possess translation symmetry and are sometimes referred to as systems with deterministic disorder. That is, these systems show some type of long-range order even though they are not periodic [43]. In 1D, this *aperiodic* order is usually encoded in sequences of symbols that can be generated using an inflation rule. The mathematical study of such structures is called symbolic dynamics [45]. That is the study of the dynamical system formed by a set of symbols subjected to the repeated application of a function that maps the set of symbols to the set of combinations of symbols.

We consider finite-size words $W \in V$, where V denotes the set of finite words that can be generated from an alphabet $\mathcal{A} = \{a_0, a_1, \dots, a_m\}$ of inequivalent symbols. These words can be constructed by repeatedly applying a substitution rule $\sigma : \mathcal{A} \rightarrow V$. The substitution rule imposes recurrence relations on words, which makes it easy to generate them. Suppose one starts with the “seed” letter a_0 . We call the word *uniquely* generated by applying the rule σ to the seed letter N times the N^{th} approximant of the aperiodic sequence. Below, we give a few examples of aperiodic sequences that we use throughout this work.

a. Fibonacci sequence. The Fibonacci words can be generated from the binary alphabet $\mathcal{A} = \{A, B\}$ by applying the following recursion relation,

$$W_N = W_{N-1}W_{N-2}, \text{ for } N > 1, \\ W_0 = A, W_1 = AB,$$

In the above equation, the product of words means that they are concatenated. This is an example of a 1D quasicrystal, as it can be obtained via a cut-and-project scheme from a regular 2D square lattice [46].

b. Tribonacci sequence. The Tribonacci word is an extension of the Fibonacci word, and it is also a quasicrystal. However, its cut-and-project scheme results from a 3D cubic lattice instead [47]. The alphabet generating the word is composed of three letters $\mathcal{A} = \{A, B, C\}$, and the recursive scheme to generate the word is

$$W_N = W_{N-1}W_{N-2}W_{N-3}, \text{ for } N > 2, \\ W_0 = A, W_1 = AB, W_2 = ABAC.$$

c. Thue-Morse sequence. The two previous words are examples for which the Pisot substitution conjecture holds [48, 49]. The characteristic matrix of the substitution dynamics has a polynomial of degree equal to its

dimension. This makes their diffraction spectrum pure-point. It is for this reason that they can be called quasicrystals [46]. The Thue-Morse chain is not generated by a Pisot substitution and is an example of an aperiodic chain that is not a quasicrystal. It has a singular-continuous diffraction spectrum [50]. The sequence is generated by repeatedly applying the substitution rule $\sigma(A) = AB$ and $\sigma(B) = BA$ to the binary alphabet. Alternatively, it can be generated by the following recurrence relation

$$W_N = W_{N-1}\overline{W_{N-1}}, N > 0, \\ W_0 = A,$$

where $\overline{W_N}$ is the bit-wise negated word: $A \rightarrow B$ and $B \rightarrow A$. That is, the N generation word is obtained by concatenating the $N-1$ generation word with its bit-wise negated version.

d. Rudin-Shapiro sequence. Finally, the last example of an aperiodic chain that we investigate is the Rudin-Shapiro chain [51]. This system is different from the previous three in the sense that it features an absolutely continuous diffraction spectrum. In order to generate the binary Rudin-Shapiro sequence, we use the following two-step procedure: We first impose the substitution rule on the four-letter alphabet $\mathcal{A} = \{A, B, C, D\}$:

$$\sigma : \begin{cases} A \mapsto AB, \\ B \mapsto AC, \\ C \mapsto DB, \\ D \mapsto DC. \end{cases}$$

This is then followed by the second step, which identifies $A, B \rightarrow A$, and $C, D \rightarrow B$. In this way, starting with the seed A , we obtain the Rudin-Shapiro binary sequence, which starts as $AAABAABAAAABBBAB\dots$

Next, we provide a brief review of the literature on the nature of topological phases observed in the last decade for a particular subset of aperiodic systems, namely, quasicrystals.

IV. THE NATURE OF TOPOLOGICAL PHASES OF QUASICRYSTALLINE INSULATORS

We will first briefly describe a few experimental realizations that show topology, after which we focus on two main concepts that are essential to understand the classification of these systems: dimensional extension and topological charge pumping.

Three experimental realizations are especially noteworthy [16, 20, 38]. In Ref. [38], the authors observed topological properties of quasicrystals using photonic waveguides to simulate a tight-binding Hamiltonian. The dependence on the phason angle of the quasicrystal was used to detect “topological phase transitions”. That is, they smoothly interpolated between two quasiperiodic chains and observed a closing of the gap whenever the

topological gap labels on either side of the interface were distributed differently. These observations can be interpreted as topological phase transitions between phases characterized by different bulk properties.

On the other hand, Refs. [16, 20] studied boundary properties of the quasicrystals through pumping procedures, which make boundary modes traverse bulk gaps after a pumping cycle has been completed. Specifically, in Ref. [16], light was topologically pumped across a system of coupled single-mode waveguides. The change in quasiperiodic modulation was driven by ϕ , the phason angle, by varying the distance between the waveguides along the propagation direction z . This effectively parametrizes the Hamiltonian as $H[\phi(z)]$, which is then used to perform an adiabatic pumping cycle. The quasicrystal in this work was constructed using the André-Aubry-Harper model, which contains a cosine modulation of the potential incommensurate with the lattice. In Ref. [20], on the other hand, photonic topological pumping was realized for a discrete Fibonacci quasicrystal. This was possible because of a topological equivalence between the two models, implemented by a potential that smoothly interpolates between the two limits [15]. This potential was used to construct a generalized experimental setup, which allowed to study the equivalence of the topological gaps and the pumping across them.

Given that the experimental observations of the topological properties of quasicrystals rely on a dimensional extension, we will focus on describing it in more detail.

A. Chern Numbers from 2D parent Hamiltonian

The André-Aubry-Harper model is represented by a tight-binding Hamiltonian in 1D, where the on-site potential (or the hopping parameter) is modulated by a periodic function, whose period is incommensurate with the lattice. For a system with on-site modulation, the Hamiltonian is

$$H(\phi) = -g \sum_j c_j^\dagger c_{j+1} + \sum_j V_j(\phi) c_j^\dagger c_j + \text{h.c.}, \quad (3)$$

where g is the hopping parameter, $c_j^{(\dagger)}$ is the annihilation (creation) operator of an electron at site $x_j = ja$, and $V_j(\phi) = V_0 \cos(2\pi\tau x_j + \phi)$, with V_0 the strength of the on-site potential and τ the incommensurate period, i.e. some irrational number.

The topological properties associated to the gaps of this 1D model may be obtained due to the residual phason degree of freedom ϕ , which makes the potential $V_j(\phi)$ be 2π -periodic, and allows for a dimensional extension to a 2D parent Hamiltonian. Interpreting ϕ as the momentum k_y in the orthogonal direction to the 1D chain, one

obtains the 2D parent Hamiltonian

$$\mathcal{H} = \sum_{m,n} \left(g c_{m,n}^\dagger c_{m+1,n} + V_0 \frac{e^{2\pi i \tau m}}{2} c_{m,n}^\dagger c_{m,n+1} + \text{h.c.} \right). \quad (4)$$

This is the well-known Hofstadter Hamiltonian of a rectangular lattice in the presence of a uniform magnetic field, with τ flux quanta per unit cell [52]. Now, $c_{m,n}^{(\dagger)}$ is the annihilation (creation) operator of an electron in a site labelled by two integers (m, n) , corresponding to the coordinates on a 2D lattice. When using a rational approximant $\tau_d = p_d/q_d$, with $p_d, q_d \in \mathbb{Z}$, it is possible to analyze the problem using magnetic translation groups, and calculate the band structure of the magnetic BZ [53]. The unit cell is q_d times smaller than the real space one, and as such, one obtains q_d bands. There is a Chern number associated to each one of those bands [54],

$$C_l = \int \frac{dk_x dk_y}{2\pi} F_{xy}^{(l)}(\mathbf{k}), \quad l \in \{1, \dots, q_d\}, \quad (5)$$

where $F_{xy}^{(l)}(\mathbf{k}) = \partial_x \mathcal{A}_y^{(l)} - \partial_y \mathcal{A}_x^{(l)}$ is the Berry curvature, $\mathcal{A}_\alpha^{(l)}(\mathbf{k}) = \langle u_l(\mathbf{k}) | \partial_\alpha | u_l(\mathbf{k}) \rangle$ is the Berry connection, and $|u_l(\mathbf{k})\rangle$ is the Bloch state corresponding to the l^{th} band. This topological quantity is proportional to the Hall conductivity σ_H of an electronic system at a certain filling characterized by an integer l_F , corresponding to the last band below the Fermi energy E_F [54]:

$$\sigma_H = \frac{e^2}{h} \sum_{l \leq l_F} C_l.$$

In this case, the bulk-boundary correspondence tells us that the Hall conductivity is generated by the conducting channels associated to the chiral, gapless edge states.

Going back to the 1D quasicrystal, it turns out that the Berry curvature is independent of the phason degree of freedom ϕ , therefore allowing the Chern numbers to be identified with the gap labels of the chain [16]. However, the notion of bulk-boundary correspondence is only recovered by sweeping through ϕ , as it forces boundary modes to cross the bulk gaps. This is a universal feature of topological charge pumps, independent of the model considered, and is even robust in the presence of electronic interactions and disorder [55]. The absence of anti-unitary symmetries protecting the topology of the system is responsible for this robustness. It was also recently shown that topological charge pumping is possible in a variety of aperiodic systems when their bulk gaps stay open throughout the pumping cycle [56].

Finally, we note that when $\tau = (\sqrt{5} - 1)/2$ (in units of the lattice constant a), which is the inverse of the golden ratio, the Hamiltonian Eq. (3) is topologically equivalent to the Fibonacci Hamiltonian, obtained by a discrete Sturmian sequence replacing the on-site potential: $V_j(\phi) \rightarrow v_j = \pm 1$ [33]. The Fibonacci word is generated by the discrete function

$$v_j = 2 \left(\left\lfloor \frac{j+2}{\tau} \right\rfloor - \left\lfloor \frac{j-1}{\tau} \right\rfloor \right) - 1 = \pm 1.$$

This equivalence is based on the generalized interpolating Harper-Fibonacci (HF) potential function [15]

$$V_{\text{HF}}^{(\beta)}(x_j, \phi) = \frac{\tanh\{\beta[\cos(2\pi\tau x_j + \phi) - \cos(\pi\tau)]\}}{\tanh\beta}, \quad (6)$$

for which the $\beta \rightarrow 0$ limit corresponds to the Harper modulation, and the $\beta \rightarrow \infty$ limit to the Fibonacci modulation. As a consequence, the Fibonacci chain shares the topological properties of the André-Aubry-Harper model. This specific insight allowed to experimentally verify that the critical states of the Fibonacci chain emerge through a cascade of localization-delocalization transitions [40].

V. TOPOLOGICAL CHARGE PUMPING OF APERIODIC SYSTEMS

The idea of topological charge pumping dates back to an argument made by Laughlin to explain the robustness of the quantized conductance in a two-dimensional quantum Hall system [57]. Soon thereafter, Thouless showed, using similar arguments, that particle transport in a 1D system subjected to an adiabatic evolution will obey the same quantization condition [58]. Because charge pumping is analogous to the Quantum Hall phase in 2D, where a quantized amount of charge is pumped on the boundary of a cylinder upon the insertion of one flux quantum [54, 57], this provides an intuitive understanding of the dimensional extension performed in Section IV A.

The dimensional extension achieved with the 2D parent Hamiltonian representation reveals that the topological classification enjoyed by the 1D quasicrystalline insulator is equivalent to the 2D class *A* of the ten-fold way [22]. It is the most robust class, as it is devoid of any symmetry. As long as the perturbations are applied adiabatically, it is guaranteed that the system stays in the same topological phase. This is the reason why quasicrystallinity is completely irrelevant to the topological classification of a 2D time-reversal-symmetry-breaking insulator.

In fact, recent work has shown quantized topological charge transport in a periodically modulated (in time) 1D Fibonacci quasicrystal [21]. A Rice-Mele [59] pump with a Fibonacci modulation of the potentials displays the interesting possibility of multilevel pumping, a feature that is not present in equivalent crystalline systems. When the modulation is quasiperiodic, the number of pumped charges is instead characterized by a Bott index [60, 61], which, in the thermodynamic limit, is equivalent to the Chern number obtained in the periodic modulation case.

In the following, we shall briefly describe how quantized charge pumping occurs in a 1D periodic crystal, and how this quantization can be ascribed to the Chern theorem.

A. Charge transport as a polarization current

Starting from a one-dimensional crystalline insulator, an adiabatic evolution of the system driven by a parameter λ induces a change in the polarization density

$$\Delta P = \int_{\lambda_i}^{\lambda_f} d\lambda \partial_\lambda P.$$

The modern theory of polarization [62] dictates that

$$\partial_\lambda P = \frac{1}{2\pi} \sum_n^{\text{occ}} \int_0^{2\pi} dk \text{Im} \langle \partial_\lambda u_n | \partial_k u_n \rangle$$

where $|u_n\rangle$ is a Bloch state corresponding to the n^{th} band of the system. If the parameter λ is periodic, i.e. the evolution is cyclic, one can identify $\text{Im} \langle \partial_\lambda u_n | \partial_k u_n \rangle = F^{(n)}(\lambda, k)$ as a Berry curvature, which means that the total change in polarization over one cyclic change of λ yields a total integral of the Berry curvature over a torus,

$$\begin{aligned} \Delta P &= \frac{1}{2\pi} \sum_n^{\text{occ}} \int_0^{2\pi} dk \oint d\lambda F^{(n)}(\lambda, k) \\ &= \sum_n^{\text{occ}} C_n \in \mathbb{Z}, \end{aligned} \quad (7)$$

where C_n denotes the Chern number of the n^{th} band [see Eq. (5)]. In the modern theory of polarization, this change in polarization can also be understood as a change in the Wannier center positions through the Berry phase formulation of the Wannier center. Therefore, Eq. (7) predicts that there is an integer amount of charges crossing the unit cell of the one-dimensional crystal. This means that, as a consequence of the Chern theorem, the total change in polarization is quantized to an integer number.

An intuitive example of a system that will also be discussed later is the Rice-Mele charge pump [59, 63]. This is a model that connects the trivial phase of the SSH model to its topological phase and back to its trivial phase in an adiabatic cycle by breaking chiral symmetry. The Rice-Mele Hamiltonian is given by

$$\begin{aligned} H(t) &= \sum_{j=1}^N [\Delta - (-1)^j \delta(t)] c_j^\dagger c_{j+1} \\ &\quad - \sum_{j=1}^N (-1)^j h(t) c_j^\dagger c_j + \text{h.c.}, \end{aligned} \quad (8)$$

where the first part is similar to the SSH model in Eq. (1), but with an independent hopping parameter Δ and a time-dependent dimerization $\delta(t)$. The second term adds a staggered on-site potential. The time-modulated functions are given by

$$\begin{aligned} \delta(t) &\equiv \delta_0 \cos(2\pi t/T), \\ h(t) &\equiv h_0 \sin(2\pi t/T). \end{aligned}$$

Here, δ_0 and h_0 are constant amplitudes, and T is the modulation period. The Bloch Hamiltonian for this system is simply given by

$$H(k, t) = \begin{pmatrix} h(t) & v_+ + v_- e^{-ik} \\ v_+ + v_- e^{ik} & -h(t) \end{pmatrix},$$

where $v_{\pm} = \Delta \pm \delta(t)$. Then, it becomes clear that at $t = 0, T$, the system is in the trivial phase of the SSH model, with $h(0) = 0$ and $v_+ > v_-$. On the other hand, at $t = T/2$, the system is in the topological phase, with $v_+ < v_-$.

B. Bott-Index formulation of quantized charge pumping

In Ref. [21], the Bott index [60, 61] was used to demonstrate quantized charge pumping for a generalized Fibonacci chain, whose on-site and hopping parameters followed the quasiperiodic modulation. We will now summarize how the Bott index is defined for charge pumping and show that it leads to the same phase diagram as the Chern number.

In its most general form, the Bott index is a measure of the total phase picked up by a string of 2D position operators (\hat{X}, \hat{Y}), projected onto the insulating ground state $|\psi\rangle$, as they complete infinitesimal loops in real space. The contribution from all such loops over the whole system yields the Bott index. More concretely, let

$$\begin{aligned} \hat{U} &= \hat{P} \exp\left(\frac{2\pi i \hat{X}}{L_x}\right) \hat{P}, \\ \hat{V} &= \hat{P} \exp\left(\frac{2\pi i \hat{Y}}{L_y}\right) \hat{P}, \end{aligned} \quad (9)$$

where L_x and L_y are the dimensions of the system in the x and y directions, respectively. The Bott index is then defined as

$$\mathcal{B} \equiv \frac{1}{2\pi} \text{Im Tr} \log \left(\hat{V} \hat{U} \hat{V}^\dagger \hat{U}^\dagger \right). \quad (10)$$

It has been shown that $\mathcal{B} = C$ in the thermodynamic limit [60], but even in the finite-size system, under periodic boundary conditions, it is a good indicator of a non-trivial topological character. Indeed, it works very well for nonperiodic 2D systems, such as disordered Chern insulators or amorphous materials [4, 5, 60]. In the case of adiabatic charge pumping, one deals with a periodic temporal parameter, which simplifies the formulation of the problem, as the Hamiltonian already comes in block diagonal form along the time axis and has instantaneous eigenstates $|\psi(t)\rangle$. It can be shown that the Bott index can be formulated in terms of a new set of operators \tilde{U}, \tilde{V} , which are obtained from Eq. (9) by understanding the action of the \hat{Y} operator on momentum eigenstates.

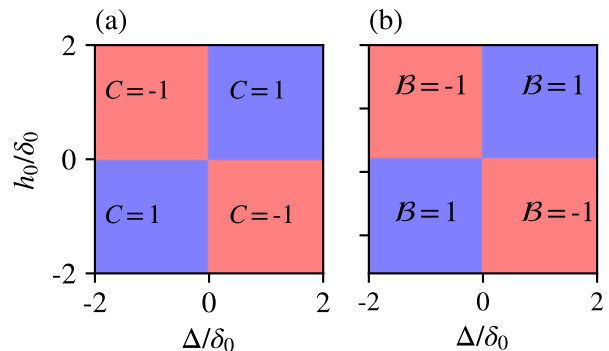


FIG. 1. Equivalence of the topological phase diagram of the periodic Rice-Mele model, at half-filling, between (a) the Chern number formulation and (b) the Bott index formulation.

These operators take the form

$$[\tilde{U}]_{mn} = \langle \psi_m(t) | \exp\left(\frac{2\pi i \hat{X}}{L_x}\right) | \psi_n(t) \rangle,$$

$$[\tilde{V}_{t,t+\Delta t}]_{mn} = \langle \psi_m(t) | \psi_n(t + \Delta t) \rangle,$$

where Δt denotes a discrete time step between adjacent times. Therefore, one can compute the Bott index as

$$\mathcal{B} = \frac{1}{2\pi} \sum_{t=0}^T \text{Im Tr} \log \left(\tilde{V}_{t,t+\Delta t} \tilde{U}_{t+\Delta t} \tilde{V}_{t,t+\Delta t}^\dagger \tilde{U}_t^\dagger \right). \quad (11)$$

In Fig. 1, one can see the equivalence of the phase diagram computed from (a) the Chern number given by Eq. (5) and (b) the Bott index given by Eq. (11).

C. Aperiodic systems

Recent work has shown quantized topological charge transport in a time-periodically modulated 1D Fibonacci quasicrystal [21]. Using Eq. (8), but modifying the periodic modulation of the dimerization and on-site potentials to a quasiperiodic one following the Fibonacci sequence, they have been able to show the possibility of multilevel pumping, a feature that is not present in equivalent crystalline systems. Multilevel pumping entails that it is possible to pump across multiple gaps simultaneously. In the Fibonacci modulation case, this can be understood from a renormalization perspective, in which gaps of different generations can be mapped to each other [21] due to the self-similar nature of the energy spectrum. In this work, we show that multilevel pumping occurs for at least two other aperiodic modulations: a Tribonacci sequence and a Thue-Morse sequence. Each one represents a different class of aperiodicity, with the Tribonacci chain being a quasicrystal obtained from projecting a 3D cubic lattice onto a line with an irrational

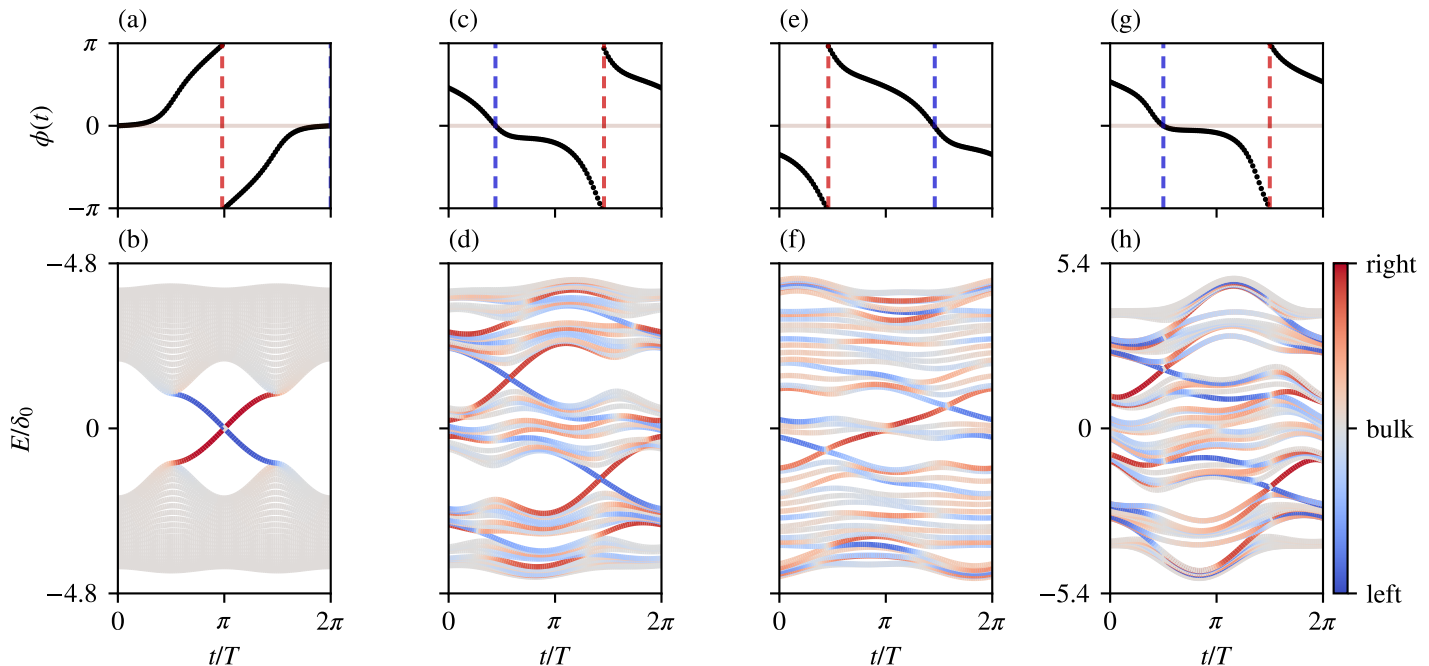


FIG. 2. Top row: time evolution of the Berry phases of each model studied under a pumping cycle. Vertical dashed lines indicate the mirror symmetric points $\phi = 0$ (blue), or $\phi = \pi$ (red). Bottom row: behavior of the eigenvalues under adiabatic time evolution. The colors indicate the localization behavior of each mode, with grey denoting bulk modes and red (blue) indicating localization on the right (left) of the chain. (a,b) Periodic Rice-Mele, (c,d) Fibonacci Rice-Mele, (e,f) Tribonacci Rice-Mele, (g,h) Thue-Morse Rice-Mele.

slope and the Thue-Morse being an aperiodic sequence not forming a quasicrystal. The Rice-Mele Hamiltonian in Eq. (8) is modified to

$$H(t) = \sum_{i=1}^N \left(\left\{ [\Delta - W_i \delta(t)] c_i^\dagger c_{i+1} + \text{h.c.} \right\} - W_i h(t) c_i^\dagger c_i \right), \quad (12)$$

where W_i is the i^{th} component of the finite approximant to an aperiodic sequence $W = \{W_1, W_2, W_3, \dots, W_N\}$, with N sites for periodic boundary conditions (PBC) and $N - 1$ sites for open boundary conditions (OBC). We will consider finite-size words $W \in V$ generated by a substitution rule, where V denotes the set of finite words that can be generated from an alphabet \mathcal{A} (see Section III).

Now, we apply the first three modulations described in Section III to the Hamiltonian Eq. (12), then numerically compute the time dependent spectra and plot the results in Fig. 2. Additionally, we also calculate the time-dependent Berry phases of the crystalline approximant in order to track the appearance of inversion symmetry, which can possibly yield a crystalline topological phase at the point where the in-gap edge modes cross and become degenerate. In Figs. 2(a) and 2(b), the results for the periodic modulation are shown. In Fig. 2(a) we see that at $t = \pi$ (in units of the period T), the Berry phase is equal to π , indicating the presence of inversion sym-

metry [8]. This result is corroborated by the crossing of the in-gap modes at $E = 0$ in Fig. 2(b). The color code of the eigenstates indicates whether they are bulk (grey)- or edge-localized (red and blue) modes. This is a visual confirmation that $t = \pi$ is the time at which the chain is in the topological phase. In Figs. 2(c) and 2(d), the same information is plotted for the Fibonacci modulation. In Fig. 2(c), one can see that the inversion symmetric points are now located near $t = \pi/2$ and $t = 3\pi/2$. In Fig. 2(d), the novel feature of multilevel pumping can be observed, as was pointed out in Ref. [21]. The reason for this behavior can be understood from a real-space-renormalization approach. The instantaneous state at the largest gap can be mapped to a state in a smaller gap, with renormalized Hamiltonian parameters. In Figs. 2(e) and 2(f), a similar behavior is observed for the Tribonacci chain, with multilevel charge pumping and inversion symmetric points appearing around $t = \pi/2$ and $t = 3\pi/2$. Finally, Figs. 2(g) and 2(h) show the results for the Thue-Morse chain, also indicating multi-level charge pumping and the appearance of inversion symmetric points concomitant with the crossing of edge modes at the largest gaps.

In order to corroborate the claims on multilevel pumping, we also calculate the amount of charge pumped at any time, which is given by the partial sum of Eq. (11),

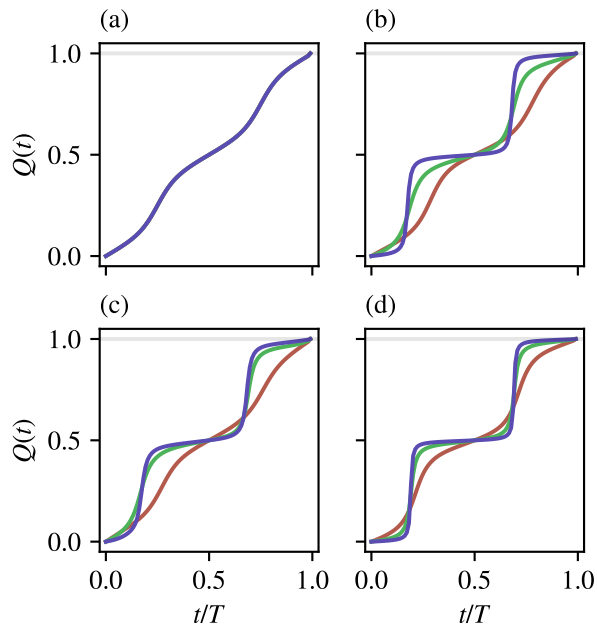


FIG. 3. Cumulative charge pumped as a function of time. (a) The periodic modulation at half-filling. (b) The Fibonacci modulation at fillings τ (red), τ^3 (green), and τ^6 (blue), with $\tau = (\sqrt{5} - 1)/2$ the inverse of the golden ratio. (c) The Tribonacci modulation at fillings η (red), η^3 (green), and η^4 (blue), with $\eta^{-1} \approx 1.8393$ the real root of the cubic equation $x^3 - x^2 - x - 1 = 0$, also called the Tribonacci constant. (d) The Thue-Morse modulation at fillings $1/3$ (red), $1/10$ (green), and $1/27$ (blue). For the aperiodic models, the behavior tends to a step-like function for smaller fillings, which is a feature of multi-level charge pumping.

i.e.

$$Q(t) = \frac{1}{2\pi} \sum_{t'=0}^t \text{Im Tr} \log \left(\tilde{V}_{t',t'+\Delta t} \tilde{U}_{t'+\Delta t} \tilde{V}_{t',t'+\Delta t}^\dagger \tilde{U}_{t',t'+\Delta t}^\dagger \right).$$

The results are shown in Fig. 3. In Fig. 3 (a), the periodic modulation is shown at half-filling, as there is only one gap. This is single-level pumping. In Figs. 3 (b) - (d), the charge pumped at three different fillings for the Fibonacci, Tribonacci, and Thue-Morse modulations is shown, respectively. In each case, we see that the charge is gradually increasing to a maximum of 1 at the end of the pumping cycle, a hallmark of quantized multilevel charge pumping. We also note that the form of the curve tends towards a step-like function for decreasing filling in all three cases, generalizing the observations made in Ref. [21].

Finally, we note that for each case, we calculated the Berry phase for a filling corresponding to the largest gap below $E = 0$. In each case, we see that $\phi(t) = \pi$ exactly where the edge modes cross, indicating that the system is in a nontrivial 1D topological phase, with an anomalous polarization of $P = 1/2$. This motivates us to investigate the realization of this phase and to study

it separately in order to show the anomalous topological response appearing at those points.

VI. TOPOLOGICAL SIGNATURES IN APERIODIC SYSTEMS

Given the considerations laid down at the end of Section V, we expect a nontrivial insulating phase in 1D, with the corresponding protected anomalous boundary responses at exactly the points where the finite approximants show inversion symmetry. It remains challenging though, to show any bulk-boundary correspondence for a true aperiodic system (of infinite size), as the concept of a unit cell possessing inversion symmetry breaks down. Moreover, it was shown that is possible to adiabatically transform a quasiperiodic system, such that the open chain has its edge states pushed into the bulk. Thereby, one may identify the phases as being topologically equivalent to the trivial insulator [17, 42], which renders these topological phases very fragile. This is a common feature of 1D topological insulators, as even the SSH chain requires the presence of both chiral and inversion symmetries to be topologically protected. As soon as chiral symmetry is lifted, one can adiabatically deform the Hamiltonian to a trivial phase, as exemplified by the Rice-Mele charge pumping procedure.

In the following, we will show the existence of these fragile topological phases by using two typical signatures of nontrivial topology in 1D, which do not require the calculation of bulk topological invariants. The first one is the polarization response of an open system, and the second one is the ES degeneracy.

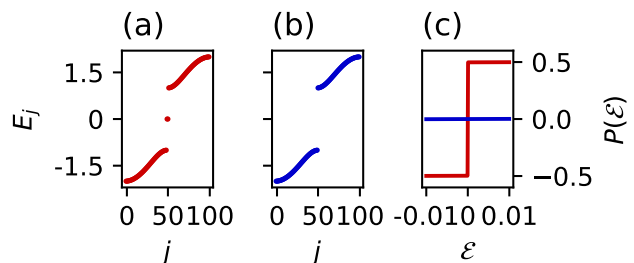


FIG. 4. Energy and polarization of the SSH chain. (a) The OBC spectrum of the SSH chain in the topological phase: two degenerate edge states are pinned at the Fermi energy. (b) The OBC spectrum in the trivial phase: all states belong to the bulk. (c) The two different polarization responses, in the trivial phase (blue) and in the topological phase (red). The dimerization parameter in Eq. (1) has been set to $\delta = \pm 0.5$ [$\delta < 0$ ($\delta > 0$): topological (trivial) phase].

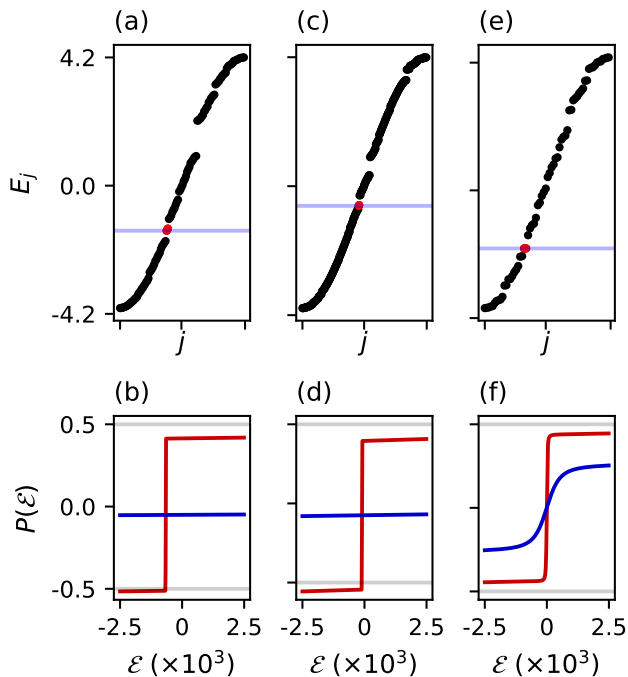


FIG. 5. Polarization response of the aperiodic chains. OBC spectra (in the nontrivial phase) and polarization responses of the (a,b) Fibonacci chain, (c,d) Tribonacci chain and (e,f) Thue-Morse chain. The fillings are chosen such that the Fermi energies (light blue line) lie in the largest gap in each case. In all cases, the polarization exhibits an anomalous behavior around $\mathcal{E} = 0$, with a jump from -0.5 to 0.5 caused by the eigenstates colored in red in (a), (c), and (e) whenever the system is in the $\phi = \pi$ phase. On the other hand, the polarization does not show a sudden jump in the $\phi = 0$ phase (in blue). All system sizes have been chosen at the same approximant level as in the charge pumping, and when needed for numerical stability, a two-unit-cell scheme was used.

A. Polarization

As a benchmark for anomalous polarization responses, we use the SSH chain introduced in Eq. (1). We expect that as soon as an infinitesimal electric field is turned on, the polarization has a value of $|P| = 0.5$ when the chain is in the topological phase. In order to probe the boundary response, we add an electric field along the chain, contributing $H_{\mathcal{E}} = \mathcal{E}\hat{X}$ to the Hamiltonian, where \mathcal{E} is the electric field strength, and the position operator is chosen to be defined as

$$\hat{X} = \sum_{m=1}^{N_c} \sum_{n=1}^{N_s} \left(-\frac{2n-1}{2N_s} - \frac{N_c}{2} + m \right) c_{m,n}^{\dagger} c_{m,n}, \quad (13)$$

where N_c is the number of cells and N_s is the number of sites in a cell. This is a generalization of the definition given in the case of the SSH chain in Ref. [9], which takes

the form

$$\hat{X} = \sum_{n=1}^N \left(-\frac{3}{4} - \frac{N}{2} + n \right) c_{2n-1}^{\dagger} c_{2n-1} + \left(-\frac{1}{4} - \frac{N}{2} + n \right) c_{2n}^{\dagger} c_{2n},$$

where N is the number of unit cells.

The position operator \hat{X} is chosen such that $x = 0$ lies at the boundary of a unit cell. Note that the total amount of sites is $L = N_s N_c$. The full Hamiltonian is then $H = H_{\text{system}} + H_{\mathcal{E}}$, where H_{system} corresponds to any system that we wish to study. The dielectric response is given by the polarization [9],

$$P(\mathcal{E}) = -\frac{1}{L-1} \sum_{n=1}^N \frac{\partial E_n}{\partial \mathcal{E}} \quad (14)$$

where $E_n \in \text{Spect}(H)$. In the limit $\mathcal{E} \rightarrow 0$, $|P|$ should agree with the polarization mentioned in Section I. In that limit, the adiabatic theorem applies, and one can choose a temporal gauge such that the minimal coupling of the electric field allows for a temporal sweep of the complete BZ [25].

More generally, using a periodic approximation for the aperiodic systems, we shall make use of Eq. (13), where each cell represents an approximant of the aperiodic structure.

a. SSH Chain. The spectra and polarization of the SSH chain are shown in Fig. 4. The OBC spectra for the topological (red) and the trivial (blue) phase are shown in Figs. 4(a) and 4(b), respectively. The anomalous response of the SSH chain in the topological phase is shown in Fig. 4(c) in red, while the response in the trivial phase is shown in blue. These results agree with the quantized Berry phase of $\phi = \pi, 0$, respectively.

b. Aperiodic Chains. We will now analyze the responses of three different aperiodic chains, each one being a representative of a different class of aperiodicity. The generic system Hamiltonian is taken from Eq. (12) at the times when the Berry phase is $\phi = \pi$ (topological) or $\phi = 0$ (trivial).

For the Fibonacci modulation, Fig. 5(a) depicts the OBC energy levels, with a choice of Fermi energy indicated by the blue line. In Fig. 5(b), the corresponding polarization $P(\mathcal{E})$ response is shown. There is a clear anomalous polarization, as indicated by the sudden jump from $P(\mathcal{E}) = -0.5$ to $P(\mathcal{E}) = 0.5$ near $\mathcal{E} \approx 0$, which is caused by the eigenstates colored in red, located at the Fermi level (light blue) in the $\phi = \pi$ phase. On the other hand, the polarization response does not show a sudden jump in the $\phi = 0$ phase (in blue). The same behavior is observed for the Tribonacci modulation in Figs. 5(c) and 5(d). For the Thue-Morse chain, in Figs. 5(e) and 5(f), we also observe a similar behavior, albeit with a trivial polarization that is not flat, but continuously increasing. We note that the results plotted in Fig. 5 do not show a

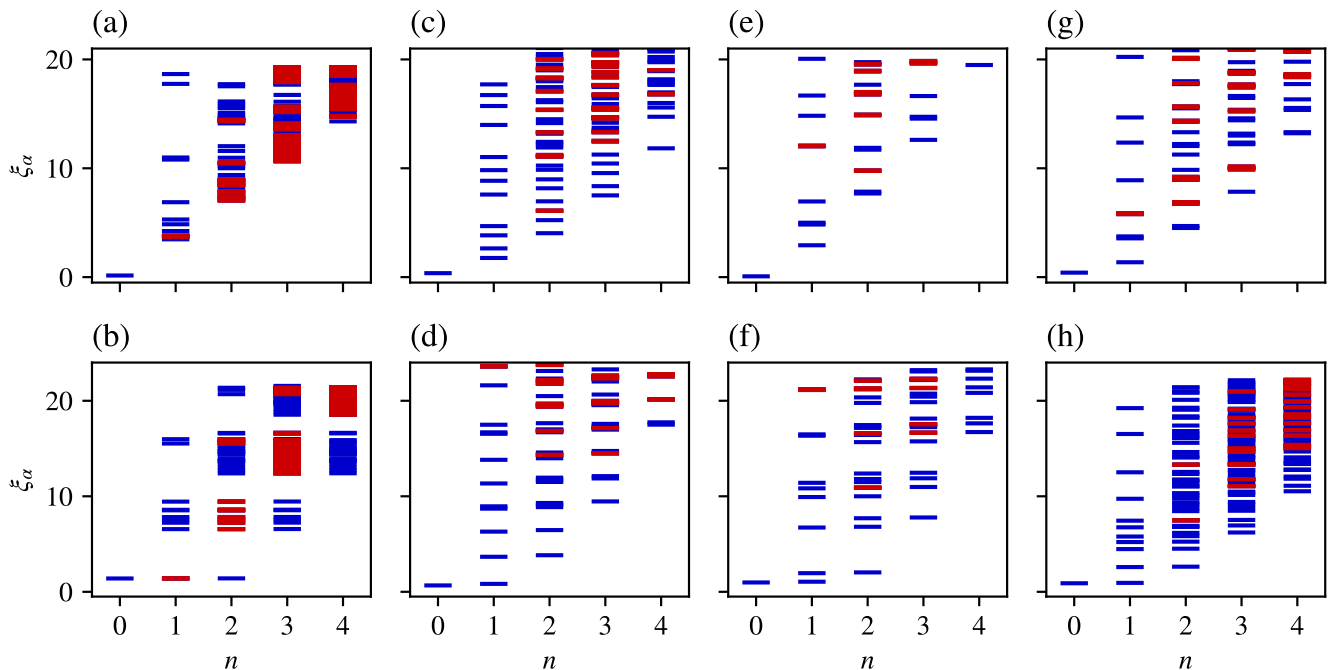


FIG. 6. First few eigenvalues of the ES plotted against the total particle number of the eigenvalue configuration. The first row indicates all the trivial realizations of the inversion symmetric chains and the lower one indicates all the topological realizations. (a,b) The SSH chain. (c,d) the Fibonacci chain. (e,f) The Tribonacci chain. (g,h) The Thue-Morse chain. A red bar indicates at least double degeneracy at the given particle number. The system sizes chosen are consistent with those computed for charge pumping and for polarization responses.

perfect equality $|P| = 0.5$ (topological), or $P = 0$ (trivial), which we suspect might be due to finite-size effects of the numerical implementation of the calculations.

B. Entanglement Spectrum

The second signature of nontrivial topological states that we will use is the degeneracy structure of the ES. There exists a one-to-one correspondence between the topological boundary modes of an open system, and the degeneracy of all eigenvalues of the ES of a subsystem taken deep in the bulk of an extended system [28]. In the following, we give a brief overview of how to calculate the ES, and the method that we used to obtain the results. We then show that the signatures of nontrivial topology are present in both the SSH chain and in the aperiodic chains.

Let us consider the ground state of a fermionic insulator, described by a quadratic Hamiltonian with a gapped single-particle spectrum. The many-body ground state of such a system is a pure product state, which can be written as

$$|\Psi_0\rangle = \prod_{n < n_F} \alpha_n^\dagger |0\rangle,$$

where the operator α_n^\dagger creates a particle in the n^{th} eigenstate of the Hamiltonian. The density matrix for this

pure state is simply given by $\rho_0 = |\Psi_0\rangle\langle\Psi_0|$. We would like to probe the entanglement between two subsystems, given a certain bipartition of the chain. Let the two systems be labeled by K and L . Then, the ES is defined to be the set of the negative logarithm of the eigenvalues of the reduced density matrix ρ_L (or equivalently ρ_K), i.e.,

$$\text{ES} = \{\xi_\alpha \in \text{Spect}(-\log \rho_L) \mid \rho_L = \text{Tr}_K \rho\}, \quad (15)$$

where Tr_K is a partial trace over the subsystem K . In the following, we will plot the ES against particle number configuration (see Appendix A for more details on how to calculate the ES).

The ES of the SSH chain is shown in Figs. 6(a) and 6(b). The difference between the trivial Fig. 6(a) and topological Fig. 6(b) phases is in the increased degeneracy of all eigenvalues in the topological phase. Restricting ourselves to the lowest eigenvalue, we see that its degeneracy goes from $D = 1$ to $D = 4$ (the red bar indicates that the degeneracy is at least of order 2). These results are already known from Ref. [64]. We shall use the degeneracy of the lowest eigenvalue as an indicator of nontrivial topological behavior at the boundary of our 1D models. In Figs. 6 (c)-(h), the ES of the aperiodic chains are shown. For each case, a double degeneracy of the lowest eigenvalue can be observed in the bottom row of the figure. Notice that since the gaps are smaller [c.f. Fig. 5], the density of eigenvalues increases, as is expected when

the system tends towards a gapless configuration. It was already known that the bulk entanglement entropy of the Fibonacci quasicrystal carries some type of signatures of the gap labels [65]. Our findings provide an indication of the nontrivial topology that could arise at the boundary when the in-gap modes are inversion-symmetric partners.

VII. CONCLUSION

The study of topological phases in quasicrystals has attracted a significant amount of attention in the last decade, and there have been many interesting experimental and theoretical observations [15, 16, 20, 29, 38]. At the same time, it is known that topological phases in 1D band insulators do not exist, except when inversion symmetry gives rise to an obstructed atomic phase. The latter results in a quantized polarization response due to fractionalized charges piling up at the boundary [13].

In this work, we put the recent observation of topological states in quasicrystals in context, and show that the charge pumps have a point in time with emergent inversion-symmetric configurations. These configurations then yield nontrivial topological phases for finite approximants of the aperiodic systems that we studied.

By calculating three typical signatures of topology in aperiodic chains, we have found genuine 1D topological phases. Namely, we have shown that the Fibonacci and Tribonacci quasicrystals and the Thue-Morse chain – representing different classes of aperiodic systems, exhibit anomalous polarization responses and that their ES possess topological eigenvalue degeneracy.

We would like to mention that our results do not hold for the Rudin-Shapiro modulation because the pumping protocol does not perform an adiabatic evolution of the system. This might be due to the different topology of the energy and Fourier spectra. It would be interesting to understand the relationship between these and the general applicability of our results. Moreover, since the results shown in this work are valid for finite realizations of aperiodic systems, it remains to verify whether these features survive in the true aperiodic limit.

ACKNOWLEDGMENTS

We would like to thank K. Dajani, L. Eek and Z. Osseweijer for fruitful discussions. This publication is part of the project TOPCORE with project number OCENW.GROOT.2019.048 which is financed by the Dutch Research Council (NWO).

-
- [1] A. P. Schnyder, S. Ryu, A. Furusaki, and A. W. W. Ludwig, Classification of topological insulators and superconductors in three spatial dimensions, *Phys. Rev. B* **78**, 195125 (2008).
 - [2] S. Ryu, A. P. Schnyder, A. Furusaki, and A. W. W. Ludwig, Topological insulators and superconductors: tenfold way and dimensional hierarchy, *New J. Phys.* **12**, 065010 (2010).
 - [3] A. W. W. Ludwig, Topological phases: classification of topological insulators and superconductors of non-interacting fermions, and beyond, *Physica Scripta* **T168**, 014001 (2016).
 - [4] A. Agarwala and V. B. Shenoy, Topological Insulators in Amorphous Systems, *Phys. Rev. Lett.* **118**, 236402 (2017).
 - [5] A. G. Grushin, Topological Phases of Amorphous Matter, in *Low-Temperature Thermal and Vibrational Properties of Disordered Solids* (WORLD SCIENTIFIC (EUROPE), 2022) pp. 435–486.
 - [6] W. P. Su, J. R. Schrieffer, and A. J. Heeger, Solitons in Polyacetylene, *Phys. Rev. Lett.* **42**, 1698 (1979).
 - [7] S.-g. Cheng, Y. Wu, H. Jiang, Q.-F. Sun, and X. C. Xie, Transport measurement of fractional charges in topological models, *npj Quantum Materials* **8**, 30 (2023).
 - [8] J. Zak, Berry’s phase for energy bands in solids, *Phys. Rev. Lett.* **62**, 2747 (1989).
 - [9] Y. Aihara, M. Hirayama, and S. Murakami, Anomalous dielectric response in insulators with the π Zak phase, *Phys. Rev. Research* **2**, 033224 (2020).
 - [10] A. Y. Kitaev, Unpaired Majorana fermions in quantum wires, *Physics-Uspekhi* **44**, 131 (2001).
 - [11] C. Brouder, G. Panati, M. Calandra, C. Mourougane, and N. Marzari, Exponential Localization of Wannier Functions in Insulators, *Phys. Rev. Lett.* **98**, 046402 (2007).
 - [12] W. Kohn, Analytic Properties of Bloch Waves and Wannier Functions, *Phys. Rev.* **115**, 809 (1959).
 - [13] B. Bradlyn, L. Elcoro, J. Cano, M. G. Vergniory, Z. Wang, C. Felser, M. I. Aroyo, and B. A. Bernevig, Topological quantum chemistry, *Nature* **547**, 298 (2017).
 - [14] C. K. Chiu, J. C. Teo, A. P. Schnyder, and S. Ryu, Classification of topological quantum matter with symmetries, *Rev. Mod. Phys.* **88** (2016).
 - [15] Y. E. Kraus and O. Zilberberg, Topological Equivalence between the Fibonacci Quasicrystal and the Harper Model, *Phys. Rev. Lett.* **109**, 116404 (2012).
 - [16] Y. E. Kraus, Y. Lahini, Z. Ringel, M. Verbin, and O. Zilberberg, Topological States and Adiabatic Pumping in Quasicrystals, *Phys. Rev. Lett.* **109**, 106402 (2012).
 - [17] K. A. Madsen, E. J. Bergholtz, and P. W. Brouwer, Topological equivalence of crystal and quasicrystal band structures, *Phys. Rev. B* **88**, 125118 (2013).
 - [18] E. Levy, A. Barak, A. Fisher, and E. Akkermans, Topological properties of Fibonacci quasicrystals: A scattering analysis of Chern numbers (2016).
 - [19] J. Bellissard, Gap Labelling Theorems for Schrödinger Operators, in *From Number Theory to Physics* (Springer Berlin Heidelberg, 1992) pp. 538–630.
 - [20] M. Verbin, O. Zilberberg, Y. Lahini, Y. E. Kraus, and Y. Silberberg, Topological pumping over a photonic Fibonacci quasicrystal, *Phys. Rev. B* **91**, 064201 (2015).
 - [21] M. Yoshii, S. Kitamura, and T. Morimoto, Topological

- charge pumping in quasiperiodic systems characterized by the Bott index, *Phys. Rev. B* **104** (2021).
- [22] A. Altland and M. R. Zirnbauer, Nonstandard symmetry classes in mesoscopic normal-superconducting hybrid structures, *Phys. Rev. B* **55**, 1142 (1997).
- [23] A. Kitaev, V. Lebedev, and M. Feigel'man, Periodic table for topological insulators and superconductors, in *AIP Conference Proceedings* (AIP, 2009) pp. 22–30.
- [24] K. G. Wilson, Confinement of quarks, *Phys. Rev. D* **10**, 2445 (1974).
- [25] B. Bradlyn and M. Iraola, Lecture notes on Berry phases and topology, *SciPost Physics Lecture Notes*, 51 (2022).
- [26] V. F. Schindler, *Higher-Order Topology in Quantum Matter*, Ph.d. thesis, University of Zurich (2021).
- [27] A. Alexandradinata, X. Dai, and B. A. Bernevig, Wilson-loop characterization of inversion-symmetric topological insulators, *Phys. Rev. B* **89**, 155114 (2014).
- [28] L. Fidkowski, Entanglement Spectrum of Topological Insulators and Superconductors, *Phys. Rev. Lett.* **104**, 130502 (2010).
- [29] J. Kellendonk and E. Prodan, Bulk–Boundary Correspondence for Sturmian Kohmoto-Like Models, *Annales Henri Poincaré* **20**, 2039 (2019).
- [30] A. B. Harris, Effect of random defects on the critical behaviour of Ising models, *Journal of Physics C: Solid State Physics* **7**, 1671 (1974).
- [31] J. M. Luck, *Journal of Statistical Physics*, Tech. Rep. (1993).
- [32] J. Hermisson, Aperiodic and correlated disorder in XY chains: exact results, *Journal of Physics A: Mathematical and General* **33**, 57 (2000).
- [33] M. Kohmoto and Y. Oono, Cantor spectrum for an almost periodic Schrödinger equation and a dynamical map, *Phys. Lett. A* **102**, 145 (1984).
- [34] J. Bellissard, B. Lochum, E. Scoppola, and D. Testard, *Commun. Math. Phys*, Tech. Rep. (1989).
- [35] C. Sire and R. Mosseri, Spectrum of 1D quasicrystals near the periodic chain, *Journal de Physique* **50**, 3447 (1989).
- [36] C. Sire and R. Mosseri, Excitation spectrum, extended states, gap closing : some exact results for codimension one quasicrystals, *Journal de Physique* **51**, 1569 (1990).
- [37] Q. Niu and F. Nori, Spectral splitting and wave-function scaling in quasicrystalline and hierarchical structures, *Phys. Rev. B* **42**, 10329 (1991).
- [38] M. Verbin, O. Zilberberg, Y. E. Kraus, Y. Lahini, and Y. Silberberg, Observation of Topological Phase Transitions in Photonic Quasicrystals, *Phys. Rev. Lett.* **110**, 076403 (2013).
- [39] A. Moustaj, S. Kempkes, and C. Smith, Effects of disorder in the Fibonacci quasicrystal (2020).
- [40] V. Goblot, A. Štrkalj, N. Pernet, J. L. Lado, C. Dorow, A. Lemaître, L. Le Gratiet, A. Harouri, I. Sagnes, S. Ravets, A. Amo, J. Bloch, and O. Zilberberg, Emergence of criticality through a cascade of delocalization transitions in quasiperiodic chains, *Nat. Phys.* **16**, 832 (2020).
- [41] A. Moustaj, M. Röntgen, C. V. Morfonios, P. Schmelcher, and C. Morais Smith, Spectral properties of two coupled Fibonacci chains, *New J. Phys.* **25**, 093019 (2023).
- [42] M. Röntgen, C. V. Morfonios, R. Wang, L. Dal Negro, and P. Schmelcher, Local symmetry theory of resonator structures for the real-space control of edge states in binary aperiodic chains, *Phys. Rev. B* **99**, 214201 (2019).
- [43] E. Maciá, The role of aperiodic order in science and technology, *Reports on Progress in Physics* **69**, 397 (2005).
- [44] A. Jagannathan, The Fibonacci quasicrystal: Case study of hidden dimensions and multifractality, *Rev. Mod. Phys.* **93** (2021).
- [45] M. Brin and G. Stuck, Symbolic dynamics, in *Introduction to Dynamical Systems* (Cambridge University Press, 2002) p. 54–68.
- [46] M. Baake and U. Grimm, *Aperiodic Order* (Cambridge University Press, 2013).
- [47] J. P. J. Krebbekx, A. Moustaj, K. Dajani, and C. Morais Smith, Multifractal properties of tribonacci chains, *Phys. Rev. B* **108**, 104204 (2023).
- [48] S. Akiyama, M. Barge, V. Berthé, J.-Y. Lee, and A. Siegel, On the Pisot Substitution Conjecture (2015) pp. 33–72.
- [49] F. Adiceam, D. Damanik, F. Gähler, U. Grimm, A. Haynes, A. Julien, A. Navas, L. Sadun, and B. Weiss, Open Problems and Conjectures Related to the Theory of Mathematical Quasicrystals, *Arnold Mathematical Journal* **2**, 579 (2016).
- [50] M. Baake, P. Gohlke, M. Kesseböhmer, and T. Schindler, Scaling properties of the thue–morse measure, *Discrete & Continuous Dynamical Systems - A* **39**, 4157 (2019).
- [51] M. Dulea, M. Johansson, and R. Riklund, Trace-map invariant and zero-energy states of the tight-binding Rudin-Shapiro model, *Phys. Rev. B* **46**, 3296 (1992).
- [52] D. R. Hofstadter, Energy levels and wave functions of Bloch electrons in rational and irrational magnetic fields, *Phys. Rev. B* **14**, 2239 (1976).
- [53] J. Zak, Magnetic Translation Group, *Phys. Rev.* **134**, A1602–A1606 (1964).
- [54] D. J. Thouless, M. Kohmoto, M. P. Nightingale, and M. den Nijs, Quantized Hall Conductance in a Two-Dimensional Periodic Potential, *Phys. Rev. Lett.* **49**, 405 (1982).
- [55] A.-S. Walter, Z. Zhu, M. Gächter, J. Minguzzi, S. Roschinski, K. Sandholzer, K. Viebahn, and T. Esslinger, Quantization and its breakdown in a Hubbard–Thouless pump, *Nat. Phys.* **19**, 1471 (2023).
- [56] J.P.J. Krebbekx, *Multifractal Properties of Tribonacci Chains*, Master thesis, Utrecht University (2023).
- [57] R. B. Laughlin, Quantized Hall conductivity in two dimensions, *Phys. Rev. B* **23**, 5632 (1981).
- [58] D. J. Thouless, Quantization of particle transport, *Phys. Rev. B* **27**, 6083 (1983).
- [59] M. J. Rice and E. J. Mele, Elementary Excitations of a Linearly Conjugated Diatomic Polymer, *Phys. Rev. Lett.* **49**, 1455 (1982).
- [60] T. A. Loring and M. B. Hastings, Disordered topological insulators via C^* -algebras, *EPL (EuroPhys. Lett.)* **92**, 67004 (2010).
- [61] M. B. Hastings and T. A. Loring, Almost commuting matrices, localized Wannier functions, and the quantum Hall effect, *Journal of Mathematical Physics* **51**, 15214 (2010).
- [62] R. D. King-Smith and D. Vanderbilt, Theory of polarization of crystalline solids, *Phys. Rev. B* **47**, 1651 (1993).
- [63] J. K. Asbóth, L. Oroszlány, and A. Pályi, *A Short Course on Topological Insulators*, Vol. 919 (Springer International Publishing, Cham, 2016).
- [64] J. Sirker, M. Maiti, N. P. Konstantinidis, and N. Sedlmayr, Boundary fidelity and entanglement in the symmetry protected topological phase of the SSH model, *Jour-*

nal of Statistical Mechanics: Theory and Experiment **2014**, P10032 (2014).

- [65] G. Rai, H. Schlömer, C. Matsumura, S. Haas, and A. Jagannathan, Bulk topological signatures of a quasicrystal, Phys. Rev. B **104**, 184202 (2021).
 [66] S.-A. Cheong and C. L. Henley, Many-body density matrices for free fermions, Phys. Rev. B **69**, 075111 (2004).

Appendix A: Entanglement Spectrum of Quadratic Hamiltonians

For quadratic Hamiltonians, it is known that the reduced density matrix takes the exponential form [66]

$$\rho_L = \det \mathcal{M}_L \exp \left[\sum_{i,j \in L} \log (G_L \mathcal{M}_L^{-1})_{ij} c_i^\dagger c_j \right],$$

where $\mathcal{M}_L = \mathbb{1} - G_L$ and $(G_L)_{ij} = \langle c_i^\dagger c_j \rangle$ is the correlation function restricted to subsystem L . Diagonalizing $G_L = M \text{diag}(\lambda_1, \dots, \lambda_n) M^{-1}$, we obtain

$$\rho_L = \exp \left[\sum_{n=1}^{|L|} \log(1 - \lambda_n) + \sum_{n=1}^{|L|} \log \left(\frac{\lambda_n}{1 - \lambda_n} \right) d_n^\dagger d_n \right],$$

where $d_n = \sum_j M_{nj} c_j$ and $|L|$ is the number of sites in subsystem L . By considering an occupation configuration of the $|L|$ fermionic eigenstates characterized by the eigenvalues of G_L , e.g. $|0, 1, 0, 0, 1, \dots, 0\rangle$, we can generate an eigenvalue of the ES. There are $2^{|L|}$ such configurations, since each of them can be either occupied or not (this is also the number of eigenvalues in the ES). Let $n_\alpha = \{0, 1, 0, 0, 1, \dots, 0\}$ be one such configuration. The corresponding ES eigenvalue is obtained through

$$\xi_\alpha = - \sum_{j=1}^{|L|} \log(1 - \lambda_j) \left[\frac{1 + (-1)^{n_\alpha^{(j)}}}{2} \right] - \sum_{j=1}^{|L|} \log(\lambda_j) \left[\frac{1 - (-1)^{n_\alpha^{(j)}}}{2} \right], \quad (\text{A1})$$

where $n_\alpha^{(j)}$ is the occupation number (0 or 1) of the j^{th} eigenstate of G_L . In order to properly visualize the spectrum, we plot it against the particle number of the occupation configuration, n_α , i.e. $n = \sum_j n_\alpha^{(j)}$.